Original Paper

American Society for Neurochemistry

ASN Neuro
Volume 10: 1–15

DOI: 10.1177/1759091418766175
journals.sagepub.com/home/asn

SAGE

Methylglyoxal Disrupts Paranodal Axoglial Junctions via Calpain Activation

Ryan B. Griggs[1], Leonid M. Yermakov[1], Domenica E. Drouet[1], Duc V.M. Nguyen[1] and Keiichiro Susuki[1]

Abstract

Nodes of Ranvier and associated paranodal and juxtaparanodal domains along myelinated axons are essential for normal function of the peripheral and central nervous systems. Disruption of these domains as well as increases in the reactive carbonyl species methylglyoxal are implicated as a pathophysiology common to a wide variety of neurological diseases. Here, using an *ex vivo* nerve exposure model, we show that increasing methylglyoxal produces paranodal disruption, evidenced by disorganized immunostaining of axoglial cell-adhesion proteins, in both sciatic and optic nerves from wild-type mice. Consistent with previous studies showing that increase of methylglyoxal can alter intracellular calcium homeostasis, we found upregulated activity of the calcium-activated protease calpain in sciatic nerves after methylglyoxal exposure. Methylglyoxal exposure altered clusters of proteins that are known as calpain substrates: ezrin in Schwann cell microvilli at the perinodal area and zonula occludens 1 in Schwann cell autotypic junctions at paranodes. Finally, treatment with the calpain inhibitor calpeptin ameliorated methylglyoxal-evoked ezrin loss and paranodal disruption in both sciatic and optic nerves. Our findings strongly suggest that elevated methylglyoxal levels and subsequent calpain activation contribute to the disruption of specialized axoglial domains along myelinated nerve fibers in neurological diseases.

Keywords

myelin, neuron-glia interaction, paranode, methylglyoxal, calpain

Received December 22, 2017; Received revised January 24, 2018; Accepted for publication February 9, 2018

Introduction

Nodes of Ranvier and associated paranodal and juxtaparanodal domains along myelinated axons form a unit essential for normal function of the peripheral and central nervous systems (PNS and CNS, respectively). Myelinating glia, Schwann cells in PNS and oligodendrocytes in CNS, are required for the formation and maintenance of this nodal functional unit. Interactions between cell-adhesion molecules (e.g., contactin-associated protein (Caspr) in axons and neurofascin (NF) 155 in myelinating glia) form axoglial junctions at paranodes. These paranodal junctions function to cluster proteins at nodes and juxtaparanodes in both PNS and CNS (Bhat et al., 2001; Boyle et al., 2001; Pillai et al., 2009; Feinberg et al., 2010; Susuki et al., 2013). Disruption of the node of Ranvier functional unit is a pathophysiology common to a wide variety of CNS and PNS diseases (for review, see Susuki, 2013; Arancibia-Carcamo and Attwell, 2014; Griggs et al., 2017b). For example, structural deficits at paranodes are found in patients with diabetic neuropathy (Sima et al., 1988a; Doppler et al., 2017), multiple sclerosis patients (Coman et al., 2006; Howell et al., 2006), or aged animals (Sugiyama et al., 2002; Hinman et al., 2006). These studies indicate that changes in the molecular structure of the nodal unit may be a cause of dysfunction in neurological diseases. The question remains, what is the pathological mediator of nodal unit disruption in the nervous system?

Several lines of evidence led to our hypothesis that the reactive carbonyl species and toxic glucose metabolite methylglyoxal disrupts the node of Ranvier functional unit in neurological diseases. First, levels of

[1]Department of Neuroscience, Cell Biology, and Physiology, Boonshoft School of Medicine, Wright State University, Dayton, OH, USA

Corresponding Author:
Keiichiro Susuki, Department of Neuroscience, Cell Biology, and Physiology, Boonshoft School of Medicine, Wright State University, 3640 Colonel Glenn Highway, Dayton, OH 45435, USA.
Email: keiichiro.susuki@wright.edu

methylglyoxal or methylglyoxal-derived advanced glycation end products are elevated in diabetic neuropathy (Bierhaus et al., 2012), multiple sclerosis (Sternberg et al., 2010, 2011; Wetzels et al., 2017), and aging (Beeri et al., 2011), all of which are associated with paranodal disruption as described earlier. Second, *in vivo* administration of methylglyoxal in rodents induces nerve conduction slowing (Bierhaus et al., 2012) or altered excitability (Shimatani et al., 2015) in sensory nerves. Third, methylglyoxal disrupts zonula occludens 1 (ZO-1) architecture in brain microvascular endothelial cells (Li et al., 2013) and decreases ezrin protein expression in renal epithelial cells (McRobert et al., 2012). Importantly, both ZO-1 (Poliak et al., 2002) and ezrin (Melendez-Vasquez et al., 2001) contribute to the molecular structure of myelin domains at nodes and paranodes. These results taken together strongly suggest that methylglyoxal could be an important mediator of nodal unit disruption in neurological diseases.

Here, we tested the hypothesis that methylglyoxal disrupts junctions formed by myelinating glial cells in the PNS and CNS. In the PNS, we found that methylglyoxal disturbed ZO-1 clusters at paranodal autotypic junctions, reduced ezrin expression in Schwann cell microvilli, and disrupted paranodal axoglial junctions. We found similar paranodal disruption in the CNS. Inhibition of calpain prevented the methylglyoxal-evoked effects on paranodal junction proteins in the PNS and CNS. Our results support the idea that disruption of nodal unit protein clusters in myelinating glia is mediated by a methylglyoxal-calpain mechanism in a wide variety of neurological diseases.

Materials and Methods

Animals

Adult male and female C57BL/6J mice (The Jackson Laboratory, Bar Harbor, ME; RRID:IMSR_JAX:000664) aged 8 to 12 weeks were used. Mice were housed in Laboratory Animal Resources at Wright State University at 22°C to 24°C under 12-hr light/12-hr dark conditions (lights on 7:00 to 19:00) with ad libitum access to water and chow. All animal procedures were approved by the Institutional Animal Care and Use Committee at Wright State University (Animal Use Protocol # 1113).

Ex Vivo Nerve Exposure

Mice were anesthetized using isoflurane inhalation and decapitated, then optic and sciatic nerves were rapidly dissected and immediately immersed in a control vehicle fluid mimicking artificial cerebrospinal fluid (aCSF). Vehicle aCSF contained (in mM): 127 NaCl, 1.8 KCl, 1.2 KH_2PO_4, 2.4 $CaCl_2$, 1.3 $MgSO_4$, 26 $NaHCO_3$, 15 glucose and was vigorously bubbled with 95% O_2/5% CO_2. All tissues were equilibrated in vehicle aCSF without drug at room temperature (22°C to 24°C) for 15 min prior to beginning drug exposure. For exposure to various doses of methylglyoxal, nerves were exposed to aCSF alone (vehicle control) or aCSF containing methylglyoxal. For exposure combining methylglyoxal and the calpain inhibitor calpeptin, nerves were exposed to aCSF containing 0.1% dimethyl sulfoxide (DMSO; vehicle control), as calpeptin stocks were initially dissolved in 100% DMSO before dilution in aCSF, and studies show that concentrations of DMSO greater than or equal to 1% may be detrimental to neuronal viability (Zhang et al., 2017). Nerves were exposed to vehicle or drug(s) at room temperature using scintillation vials in a volume of 20 mL for 6 hr. This time point was chosen based on a previous experiment indicating that 6 hr was sufficient for another reactive carbonyl species, acrolein, to induce paranodal disruption in CNS white matter after *ex vivo* exposure (Shi et al., 2011). After the exposure period, tissues were immediately fixed in 4% paraformaldehyde or snap frozen in liquid nitrogen and stored at −80°C for further processing.

Immunofluorescent Imaging and Quantification of Paranodal Disruption

Immunostaining of optic and sciatic nerve sections or teased sciatic nerves was performed as described previously (Otani et al., 2017). In brief, after the completion of methylglyoxal exposure, nerves were immediately fixed in ice-cold 4% paraformaldehyde in 0.1 M phosphate buffer for 30 min, cryoprotected overnight in 20% sucrose, blocked and placed in custom-made foil blocks, and frozen in Optimal Cutting Temperature (O.C.T.) Compound (4583, TissueTek, Sakura Finetek USA, Torrance, CA) and stored at −80°C. Optic (10 μm) and sciatic (16 μm) nerve sections were cut using a cryostat (HM550, Thermo Scientific, Waltham, MA), collected in ice-cold 0.1 M phosphate buffer, and mounted on gelatin-coated (1%) coverslips. Some fixed sciatic nerves were gently teased apart using #7 fine forceps and spread on gelatin-coated coverslips. Sectioned or teased nerves were then blocked for 1 hr in 0.1 M phosphate buffer (pH 7.4) containing 0.3% Triton X-100 and 10% goat serum (PBTGS) then incubated overnight at 4°C with primary antibodies diluted in PBTGS. Samples were washed three times for 10 min in PBTGS, followed by incubation in the dark with fluorescently labeled secondary antibodies for 1 hr at room temperature. Finally, immunolabeled samples were washed in PBTGS, 0.1 M phosphate buffer, 0.05 M phosphate buffer, air-dried, and mounted onto slides using mounting medium (Product Code 71-00-16, KPL, Geithersburg, MD). Images were captured on an Axio Observer Z1 with Apotome 2 fitted with a Axiocam Mrm CCD camera (ZEISS, Thornwood, NY). Image

analyses were performed using ZEN 2.3 software (Zeiss). The following primary antibodies were used: mouse monoclonal ankyrinG (N106/36, UC Davis/NIH NeuroMab Facility Cat# 75-146 RRID:AB_10673030), Kv1.2 (K14/16, UC Davis/NIH NeuroMab Facility Cat# 75-008 RRID:AB_2296313), pan-Nav (K58/35, Sigma-Aldrich Cat# S8809 RRID:AB_477552), ZO-1 (1A12, Thermo Fisher Scientific Cat# 33-9100 RRID: AB_2533147), ezrin (3C12, Santa Cruz Biotechnology Cat# sc-58758 RRID:AB_783303), βII spectrin (BD Biosciences; RRID: AB_399853), rabbit Caspr (Abcam Cat# ab34151 RRID:AB_869934), βIV spectrin (M.N. Rasband, Baylor College of Medicine; Texas; USA Cat# bIV SD RRID:AB_2315634), gliomedin (kindly provided by Dr. Elior Peles, Weizmann Institute of Science, Rehovot, Israel), dystrophin-related protein 2 (DRP2; kindly provided by Dr. Peter J. Brophy, Centre for Neuroscience Research, University of Edinburgh, Edinburgh, UK), and chicken polyclonal NF (R&D Systems Cat# AF3235 RRID:AB_10890736). Alexa Fluor (594, 488, 350) or AMCA conjugated secondary antibodies were used (Jackson ImmunoResearch Laboratories, West Grove, PA).

Paranodal disruption (%) was determined as previously reported (Otani et al., 2017) with minor modifications as follows. Approximately 100 nodal units from three to five images of sciatic or optic nerve sections for each nerve were randomly chosen for observation and evaluated as normal or disrupted. Next, we calculated the percentage of paranodal disruption by dividing the number of nodal units that appeared disrupted by the total number of nodal units that were observed.

Calpain Activity Assay

A Calpain Activity Assay Kit (Abcam, Cat# ab65308) was used to quantify relative calpain enzyme activity. At the end of the *ex vivo* exposure, sciatic nerves were transferred to BioMasher tubes (Takara Bio USA), snap frozen in liquid nitrogen, and stored at −80°C. Immediately prior to performing the calpain activity assay, sciatic nerves were pulverized using a pestle (BioMasher, Takara Bio USA) under liquid nitrogen and then ice-cold extraction buffer was added. Samples were centrifuged at 4°C at $21{,}000 \times g$ for 5 min. Supernatants were transferred to a fresh, ice-cold tube, and protein content was quantified using a Pierce BCA Protein Assay (Thermo Scientific, Cat# 23225). Calpain activity was measured in 25 to 50 μg of total protein for each sample according to manufacturer protocol. Changes in relative fluorescent units were detected using a Synergy H1 microplate reader (BioTek Instruments). Relative fluorescence units for each sample were blank-subtracted, divided by the total protein loaded, and normalized to the average of vehicle controls within each experiment. Calpain activity is reported as the percentage of vehicle control.

Statistical Analyses

Comparison of the means between two groups was performed using unpaired, homoscedastic *t*-test. Comparison of the effect of methylglyoxal and calpeptin on calpain activity, paranodal disruption, and ezrin was performed using two-way analysis of variance (ANOVA) followed by Tukey's multiple comparison correction. An alpha value of $\alpha = .05$ was used to determine statistical significance. All data were analyzed using Prism 7.0 (GraphPad, La Jolla, CA) and are presented as scatter plots with mean ± SEM.

Results

Methylglyoxal Disrupts Peripheral Nerve Myelin Structures

Since methylglyoxal can disrupt ZO-1 complex (Li et al., 2013), and ZO-1 is highly enriched at paranodal autotypic tight junctions of myelinating Schwann cells (Poliak et al., 2002), we tested if incubating wild-type mouse sciatic nerves with methylglyoxal would disrupt paranodal structures in PNS myelin. First, we incubated sciatic nerves with a relatively high concentration of methylglyoxal (10 mM) for 6 hr. This concentration was chosen to overcome the hematoneural diffusional barrier created by the intact epineurium, perineurium, and endoneurium in sciatic nerve explants (Villegas et al., 2014). We found that clusters of Schwann cell proteins at paranodes were frequently disorganized after exposure to methylglyoxal, but not in nerves exposed to vehicle control. The immunostaining of NF155 at paranodal axoglial junctions was absent at the paranodal region next to the nodes, whereas the clusters of axonal cell adhesion molecule NF186 were mostly preserved (Figure 1(a)). At paranodes with disrupted NF155, ZO-1 immunostaining was also reduced and disorganized (Figure 1(a)). Next, we analyzed clusters of the cytoplasmic protein ezrin localized in Schwann cell microvilli at the perinodal area surrounding PNS nodes (Melendez-Vasquez et al., 2001), since methylglyoxal decreases ezrin protein expression (McRobert et al., 2012). We found that the immunostaining of ezrin was dramatically reduced or absent in sciatic nerves exposed to methylglyoxal (Figure 1(b)). The frequency of nodal units containing normal-appearing ezrin clusters was reduced by methylglyoxal ($25.4 \pm 1.9\%$, mean ± SEM, $n = 3$ nerves) compared with vehicle control ($92.7 \pm 1.4\%$, mean ± SEM, $n = 3$; $p < .0001$, unpaired *t*-test). Similarly, methylglyoxal altered clusters of gliomedin, a protein secreted from Schwann cells and incorporated

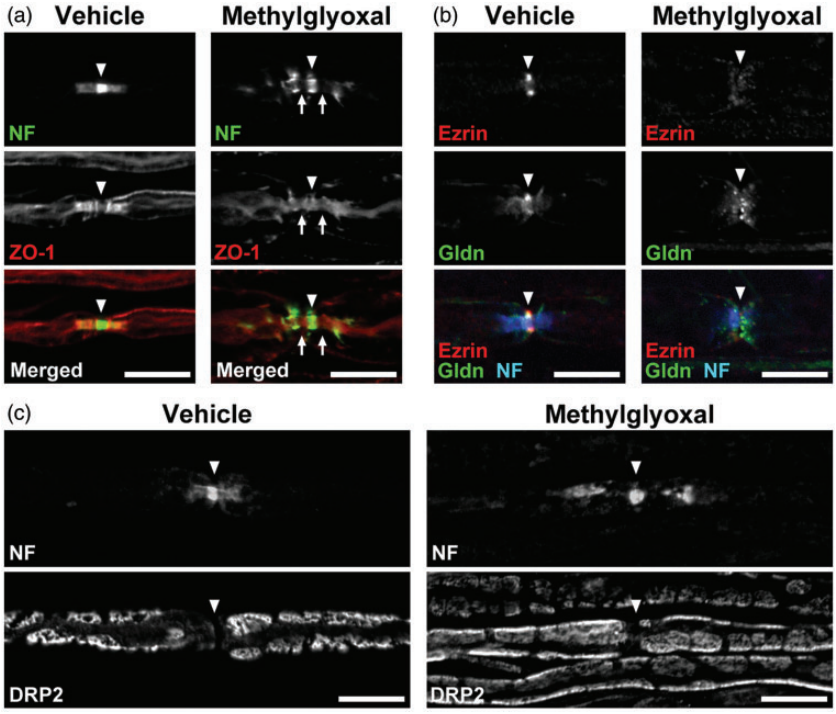

Figure 1. Myelinating Schwann cell structures are disorganized by increasing methylglyoxal. (a) In sciatic nerves exposed to vehicle control, a pan neurofascin (NF) antibody strongly labels axonal NF186 at the nodal axolemma (arrowheads), and weakly labels Schwann cell NF155 at paranodes. ZO-1 is enriched at paranodes (Vehicle, left column). After 6 hr of methylglyoxal (10 mM) exposure, both NF155 and ZO-1 staining are reduced (arrows) and disorganized at paranodes (methylglyoxal, right column). Scale bars = 10 μm. (b) Both ezrin and gliomedin (Gldn) are highly enriched at the perinodal area that surrounds nodal clusters (vehicle, left column). After methylglyoxal exposure (methylglyoxal, right column), ezrin staining is remarkably reduced and gliomedin is slightly altered (arrowhead). Scale bars = 10 μm. (c) Dystrophin-related protein 2 (DRP2) immunostaining shows characteristic cobble stone-like pattern on the myelin surface (vehicle, left column). After methylglyoxal exposure, DRP2 staining appears normal, whereas paranodal NF155 clusters are reduced and disorganized (methylglyoxal, right column). Arrowheads indicate nodal clusters. Upper panels are focused on the axon, and lower panels are focused on the outer surface of the myelin sheath. Scale bars = 10 μm.

into extracellular matrix at the PNS perinodal region (Eshed et al., 2007). Methylglyoxal exposure reduced the frequency of normal-appearing gliomedin clusters ($63.8 \pm 8.2\%$, mean ± SEM, $n = 3$ nerves) compared with vehicle ($91.3 \pm 4.4\%$, mean ± SEM, $n = 3$; $p = .04$, unpaired t-test). To test if these paranodal changes were secondary to myelin damage, we analyzed DRP2, a marker for the surface of compact myelin in PNS. The signal intensity and characteristic cobble stone-like pattern of DRP2 immunostaining were preserved in 131 of 142 (92.3%, $n = 3$ nerves) myelin sheaths associated with disorganized NF155 clusters (Figure 1 (c)). These findings suggest that paranodal structures are vulnerable to disruption by methylglyoxal, even when the overall internodal structure of the myelin sheath appears intact.

Methylglyoxal Disrupts Paranodal Axoglial Junctions in Peripheral Nerve

Our current results indicate that methylglyoxal disrupts clusters of Schwann cell proteins involved in paranodal junctions (i.e., NF155 and ZO-1). Ablation of Schwann cell NF155 leads to loss of the axonal proteins contactin and Caspr and disruption of the paranodal cell adhesion complex comprising paranodal axoglial junctions in the PNS (Pillai et al., 2009). Therefore, we tested whether paranodal axoglial junctions containing Caspr and NF155 were disrupted by methylglyoxal. In addition, to more closely mimic physiological concentrations of methylglyoxal in human plasma that range from 123 nM to 407 μM (Rabbani and Thornalley, 2014), we tested the effect of additional concentrations of methylglyoxal on paranodal junctions by exposing sciatic nerves to 1 μM, 100 μM, or 10 mM methylglyoxal for 6 hr. Immunostaining of both Caspr and NF155 was almost completely absent in some paranodes at regions nearest the node, whereas the staining was preserved near juxtaparanodes (Figure 2(a)). The nodal gap, or the distance between Caspr clusters within a nodal unit, appeared elongated after methylglyoxal exposure (Figure 2(a)). Methylglyoxal increased the frequency

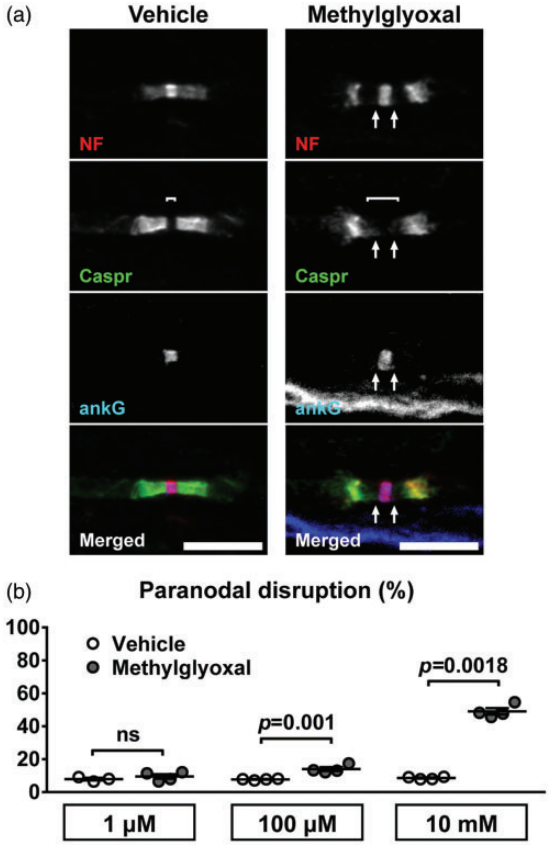

Figure 2. Methylglyoxal disrupts paranodal axoglial junctions in the PNS. (a) In sciatic nerves exposed to vehicle control for 6 hr, paranodal clusters of NF155 in Schwann cells and axonal Caspr appeared normal (left column). Methylglyoxal (10 mM) exposure resulted in elongation of the nodal gap (brackets) and paranodal disruption, characterized by a space between normal appearing nodal clusters containing axonal NF186 and ankyrinG (ankG) and paranodal axoglial clusters containing Schwann cell NF155 and axonal Caspr (arrows, right column). Scale bars = 10 µm. (b) Quantification of the percentage of nodal units exhibiting paranodal disruption in nerves treated with vehicle or methylglyoxal for 6 hr (three unpaired *t*-tests for three experiments testing three different concentrations, n=3–4 nerves per experiment). Methylglyoxal dose-dependently increased paranodal disruption. ns = not significant.

of loss of Caspr and NF155 immunostaining at concentrations of 10 mM and 100 µM, but not at 1 µM (Figure 2(b)). In multiple previous reports, loss of Caspr/NF155 immunostaining mirrored the disruption of transverse bands observed using electron microscopy (Bhat et al., 2001; Boyle et al., 2001; Pillai et al., 2009; Otani et al., 2017), suggesting that immunofluorescent results are indicative of altered fine structures at paranodal axoglial junctions. Therefore, our current results demonstrate that elevated methylglyoxal disrupts paranodal axoglial junctions in the PNS.

Axonal Clusters at Nodes and Juxtaparanodes Are Preserved After Methylglyoxal Exposure

To further test the hypothesis that paranodal clusters are the component of the nodal unit that is most susceptible to methylglyoxal-induced damage, we analyzed the effect of methylglyoxal exposure on axonal protein clustering in nodal units. Despite disorganized NF155 immunostaining at the paranode-node border, clusters of the nodal proteins ankyrinG (scaffolding protein; Figure 2(a)), Nav (ion channel), NF186 (cell adhesion molecule), and βIV spectrin (cytoskeleton) were preserved (Figure 3(a)). In nodal units with paranodal disruption induced by methylglyoxal exposure, 94 out of 95 nodal clusters appeared normal ($99 \pm 1\%$, mean ± SEM, $n = 4$ nerves). Next, we analyzed juxtaparanodal Kv1.2 expression, because loss of paranodal axoglial junctions leads to mislocalization of Kv channels into the paranodal region (Bhat et al., 2001; Boyle et al., 2001; Pillai et al., 2009). In nodal units with paranodal disruption induced by methylglyoxal exposure, 162 out of 174 juxtaparanodes contained normal-appearing Kv1.2 immunostaining ($93.0 \pm 0.4\%$, mean ± SEM, $n = 4$), without mislocalization of Kv1.2 into the paranode (Figure 3(b)). The lack of paranodal invasion of Kv1.2 was presumably due to residual diffusional barrier comprising paranodal NF155 and Caspr clusters at the region adjacent to juxtaparanodes. Furthermore, we found that the axonal cytoskeleton protein βII spectrin localized at paranodes and juxtaparanodes was preserved, despite apparent loss of NF155 in methylglyoxal-exposed nerves (Figure 3(c)). These findings support the idea that paranodes and Schwann cell microvilli are the structures of the nodal unit that are most susceptible to methylglyoxal-induced damage in myelinated nerve fibers of the PNS.

Methylglyoxal Exposure Increases Calpain Activity in Peripheral Nerve

How does methylglyoxal exposure lead to paranodal disruption? Methylglyoxal induces a wide variety of cellular pathologies including mitochondrial dysfunction (Rosca et al., 2002; Tajes et al., 2014; Chan et al., 2016; Chang et al., 2016), endoplasmic reticulum stress (Palsamy et al., 2014; Nam et al., 2015; Chan et al., 2016; Choi et al., 2016), and activation of ion channels such as transient receptor potential ankyrin 1 (Eberhardt et al., 2012; Andersson et al., 2013; Griggs et al., 2017b). Although molecularly distinct, calcium dysregulation is associated with all three of these methylglyoxal-evoked cellular pathologies, and altered calcium homeostasis results in overactivation of the calcium-dependent cysteine protease calpain (Vosler et al., 2008). Furthermore, calpain cleaves both ZO-1 (Wang et al., 2012b) and ezrin (McRobert et al., 2012), and methylglyoxal exposure

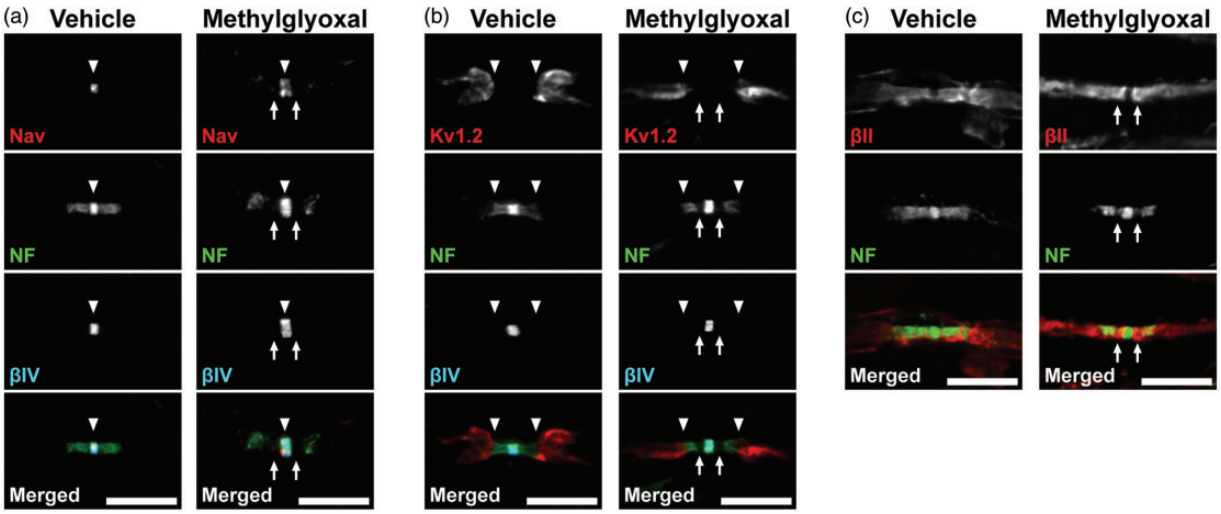

Figure 3. Axonal protein clusters are preserved after methylglyoxal exposure. (a) Nodal clusters of axonal Nav, NF186, and βIV spectrin appear normal (arrowheads) after exposing sciatic nerves to either vehicle (left column) or methylglyoxal (10 mM, right column) for 6 hr, even when associated with paranodal disruption (arrows). (b) Juxtaparanodal clusters of axonal Kv1.2 appeared normal and the paranode-juxtaparanodal border was preserved (arrowheads) after either vehicle (left column) or methylglyoxal (10 mM, right column) exposure for 6 hr. There was no evidence of Kv1.2 mislocalization to the paranode, despite methylglyoxal-evoked paranodal disruption (arrows). (c) Axonal cytoskeleton protein βII spectrin is enriched at paranodes and juxtaparanodes after either vehicle (left column) or methylglyoxal (right column) exposure for 6 hr, even when associated with paranodal disruption (arrows).

resulted in loss of both ezrin and ZO-1 (Figure 1). Thus, we hypothesized that calpain plays a role in methylglyoxal-evoked disruption of the nodal unit. To test this hypothesis, we exposed sciatic nerves to methylglyoxal (10 mM) for 6 hr and then measured calpain enzymatic activity. Compared with sciatic nerves exposed to vehicle control ($100 \pm 6.3\%$; mean $\pm$ SEM; $n = 6$ nerves), methylglyoxal exposure increased calpain activity ($167.5 \pm 9.2\%$; mean $\pm$ SEM; $n = 6$ nerves; $p < .0001$, unpaired t-test; Figure 4(a)). These data further support the idea that methylglyoxal disrupts the nodal unit via calpain activation.

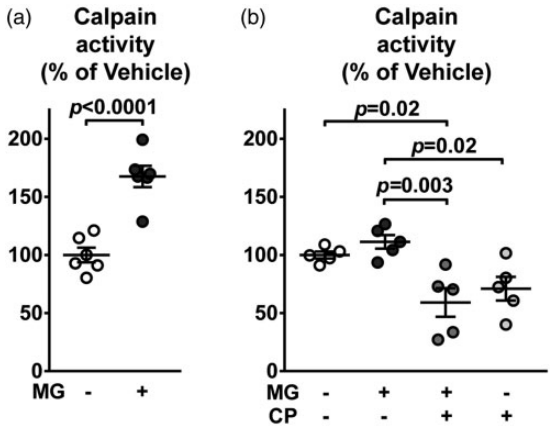

Figure 4. Methylglyoxal increases calpain activity in the PNS. (a) Exposing sciatic nerves to methylglyoxal (MG; 10 mM) for 6 hr increased calpain activity (unpaired t-test; n=6 nerves). (b) Coexposing sciatic nerves to the calpain inhibitor calpeptin (CP; 100 μM) reduced a nonsignificant increase in calpain activity evoked by methylglyoxal exposure (1 mM) alone (two-way ANOVA followed by Tukey; n=5 nerves).

Calpain Inhibition Prevents Methylglyoxal-Induced Paranodal Disruption and Ezrin Loss in PNS

To test if calpain mediates methylglyoxal-evoked disruption of paranodal (e.g., NF155, Caspr) and perinodal (e.g., ezrin) protein clusters, we coexposed sciatic nerves to methylglyoxal (1 mM) plus the calpain inhibitor calpeptin (100 μM) for 6 hr and then quantified calpain enzyme activity and immunostaining of nodal unit proteins. We chose a concentration of methylglyoxal (1 mM) that more closely resembles physiological conditions (Rabbani and Thornalley, 2014) and produces a moderate amount of paranodal disruption compared with the minimal disruption produced by 100 μM methylglyoxal (see Figure 2(b)). Previous studies indicate that 100 μM calpeptin increases neuronal survival after trimethyltin chloride treatment (Ceccariglia et al., 2011) or ameliorates kainic acid-induced decreases in GluR1 expression (Bi et al., 1998) in organotypic hippocampal slice cultures.

Compared with vehicle control ($100 \pm 3.0\%$; mean $\pm$ SEM; $n = 5$ nerves), methylglyoxal exposure produced a nonsignificant increase in calpain activity ($111.3 \pm 5.9\%$; mean $\pm$ SEM; $n = 5$; Figure 4(b)). Compared with methylglyoxal exposure alone, cotreatment with

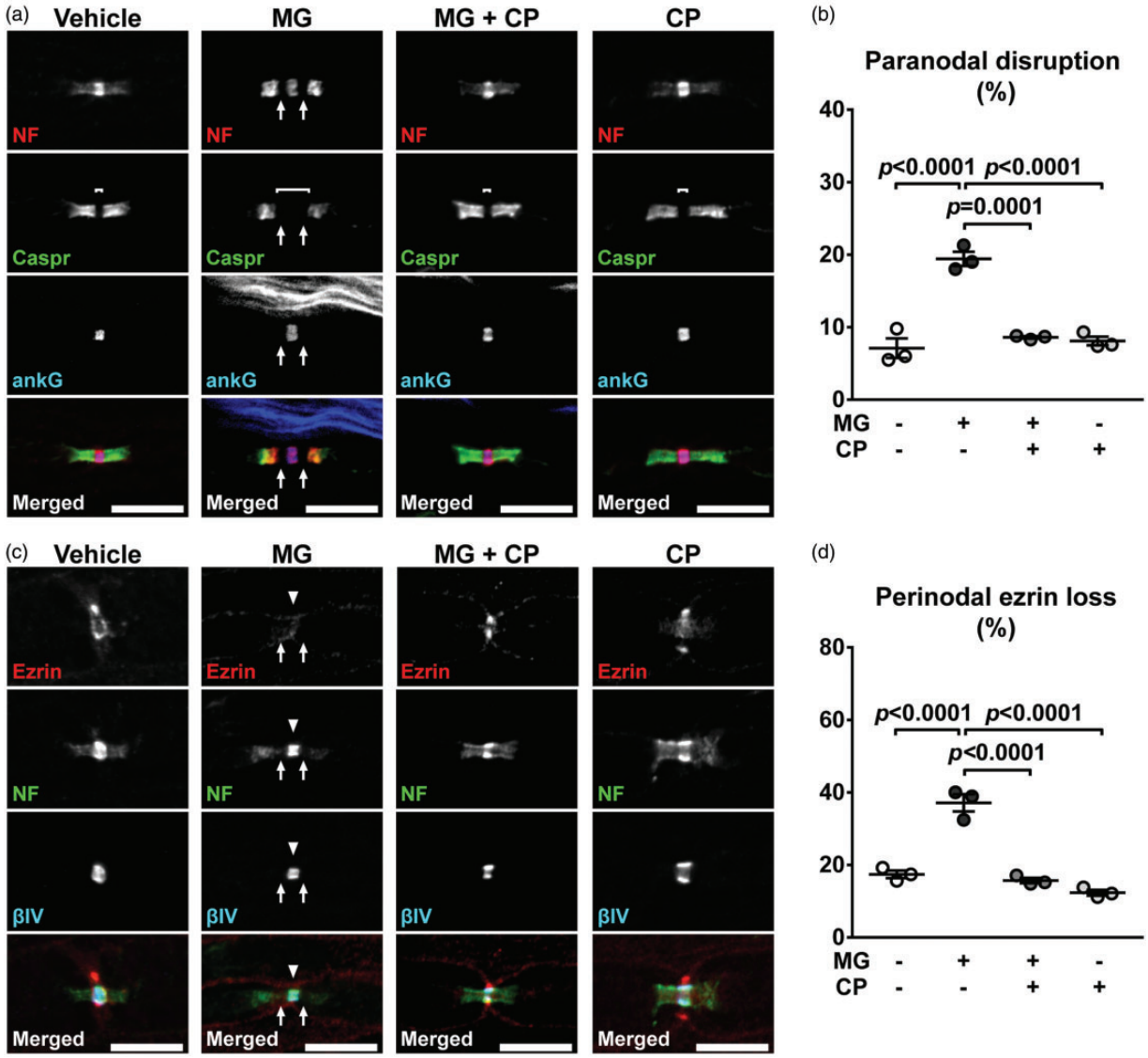

Figure 5. Calpeptin attenuates methylglyoxal-evoked paranodal and perinodal changes in the PNS. (a) Exposing sciatic nerves to vehicle for 6 hr altered neither nodal NF186 and ankyrinG (ankG) nor paranodal NF155 and Caspr immunostaining (first column). Methylglyoxal (1 mM) exposure resulted in elongation of the nodal gap (brackets) and decreased paranodal NF155 staining (arrows) adjacent to the node (MG, second column). Nodal units appeared normal after exposure to methylglyoxal plus calpeptin (MG + CP, third column). Calpeptin treatment alone did not alter the nodal unit architecture (CP, fourth column). (b) Quantification of the percentage of disrupted paranodes after exposing sciatic nerves to Vehicle, MG, MG + CP, or CP. Methylglyoxal-evoked paranodal disruption was ameliorated by calpeptin (two-way ANOVA followed by Tukey; $n=3$ nerves). (c) Sciatic nerves exposed to vehicle for 6 hr show normal nodal ezrin, NF186, and βIV spectrin, as well as paranodal NF155 immunostaining (first column). Methylglyoxal (1 mM) decreased paranodal NF155 staining adjacent to the node (arrows) and reduced ezrin labeling (arrowheads) at the perinodal area (MG, second column). Nodal units appeared normal after exposure to methylglyoxal plus calpeptin (MG + CP, third column). Calpeptin treatment alone did not alter nodal unit architecture (CP, fourth column). (d) Quantification of the percentage of perinodal ezrin loss after exposing sciatic nerves to Vehicle, MG, MG + CP, or CP for 6 hr. Methylglyoxal-evoked ezrin loss was ameliorated by calpeptin (two-way ANOVA followed by Tukey; $n=3$ nerves).

calpeptin ($59.1 \pm 12.4\%$; mean ± SEM; $n = 5$) or calpeptin exposure alone ($71.0 \pm 10.2\%$; mean ± SEM) reduced calpain activity levels ($p < .05$, two-way ANOVA followed by Tukey; Figure 4(b)). These results confirm that calpeptin reduced calpain activity in *ex vivo* sciatic nerves. Vehicle control containing DMSO did not alter the appearance of nodal or paranodal immunostaining (Figure 5(a), first column) compared with aCSF only (see Figure 2(a) and (b)). Methylglyoxal decreased paranodal NF155 and Caspr immunostaining immediately adjacent to nodal ankyrinG, resulting in the appearance of an elongated nodal gap between Caspr clusters

(Figure 5(a), second column). Simultaneous exposure to methylglyoxal and calpeptin resulted in a normal appearing nodal gap and typical paranodal NF155 and Caspr staining (Figure 5(a), third column). Calpeptin treatment alone did not alter paranodal or nodal immunostaining (Figure 5(a), fourth column). Quantification of the percentage of disrupted paranodes yielded a significant interaction between methylglyoxal and calpeptin exposure, $F(1,8) = 43.97$; $p = .0002$ (Figure 5(b)). The percentage of paranodes disrupted was greater in nerves exposed to methylglyoxal compared with vehicle control ($p < .0001$; Tukey's multiple comparison test) or calpeptin only ($p < .0001$; Tukey; Figure 5(b)). Calpeptin completely abolished methylglyoxal-evoked paranodal disruption compared with methylglyoxal treatment alone ($p = .0001$; Tukey; Figure 5(b)).

Exposure to vehicle control resulted in normal appearing ezrin immunostaining (Figure 5(c), first column). Methylglyoxal reduced perinodal ezrin immunostaining surrounding nodal βIV spectrin and NF186 (Figure 5(c), second column). Ezrin immunostaining was preserved in nerves simultaneously exposed to methylglyoxal and calpeptin (Figure 5(c), third column). Calpeptin treatment alone did not alter perinodal ezrin (Figure 5(c), fourth column). Quantification of the percentage of ezrin loss yielded a significant interaction between methylglyoxal and calpeptin treatments, $F(1,8) = 34.08$; $p = .0004$ (Figure 5(d)). The percentage of ezrin loss was greater in methylglyoxal-exposed nerves compared with vehicle control ($p < .0001$; Tukey's multiple comparison test) or calpeptin only ($p < .0001$; Tukey; Figure 5(d)). Treatment with calpeptin completely abolished methylglyoxal-evoked ezrin loss compared with methylglyoxal exposure alone ($p < .0001$; Tukey; Figure 5(d)). These data demonstrate that calpain contributes to methylglyoxal-evoked paranodal and perinodal disruption in peripheral nerves.

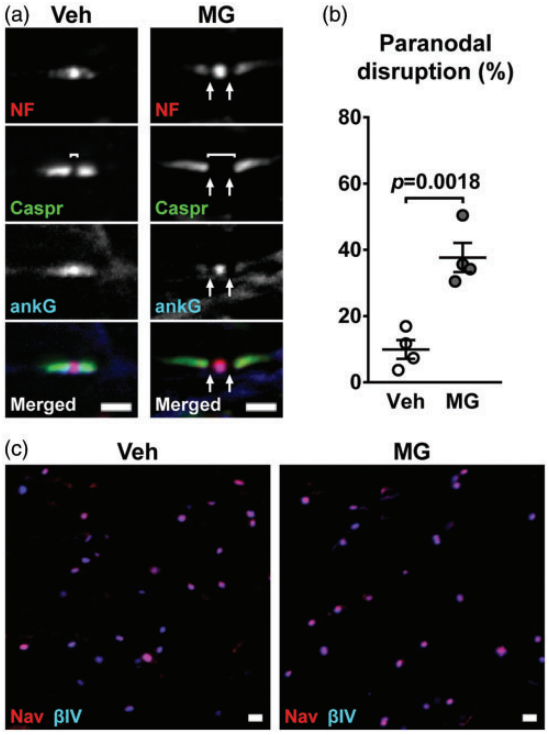

Figure 6. Elevated methylglyoxal disrupts paranodal axoglial junctions in the CNS. (a) In optic nerves exposed to vehicle control for 6 hr, paranodal clusters of NF155 in oligodendrocytes and axonal Caspr appeared intact (Veh, left column). Methylglyoxal (10 mM) exposure reduced NF155, Caspr, and ankyrinG (ankG) staining at paranodes next to the node (arrows) and resulted in nodal gap (brackets) elongation (MG, right column). Scale bars = 2 μm. (b) Quantification of paranodal disruption. Methylglyoxal increased the percentage of nodal units exhibiting loss of paranodal NF155 and Caspr adjacent to the node (unpaired *t*-test; *n*=4 nerves). (c) Representative images depicting the nodal density, or the number of Nav+ and βIV spectrin+ nodes per field of view, after vehicle (Veh; left) or methylglyoxal (MG; right) exposure. Methylglyoxal did not change the density of nodal clusters. Scale bars = 2 μm.

Methylglyoxal Disrupts Paranodal Axoglial Junctions in Optic Nerves

In addition to its pathological role in diseases of the PNS (e.g., diabetic neuropathy), methylglyoxal is implicated in CNS afflictions such as Alzheimer's (Kuhla et al., 2005). Furthermore, paranodal and nodal structures are altered in diabetic optic neuropathy (Kamijo et al., 1993). Therefore, we tested the hypothesis that methylglyoxal disrupts paranodal axoglial junctions in myelinated axons of the CNS. We exposed optic nerves to vehicle or methylglyoxal (10 mM) for 6 hr in the same *ex vivo* preparation. Similar to sciatic nerves (see Figure 2(a)), exposure of optic nerves to methylglyoxal led to loss of paranodal proteins NF155 and Caspr adjacent to nodal clusters (Figure 6(a)). The nodal gap, or the distance between Caspr clusters, appeared longer (Figure 6(a)). The percentage of paranodes that were disrupted by methylglyoxal ($37.68 \pm 4.38\%$, mean ± SEM, $n = 4$) was greater than in optic nerves exposed to vehicle only ($9.92 \pm 2.84\%$, mean ± SEM, $n = 4$; $p = .0018$, unpaired *t*-test; Figure 6(b)). We quantified the number of nodes per field of view that were immunopositive for both Nav and βIV spectrin (Figure 6(c)) and found that the nodal density was similar between vehicle (289.9 ± 22.2) and methylglyoxal (305.6 ± 9.4) exposed optic nerves ($p = .54$, unpaired *t*-test). Preservation of axonal components at nodes—NF186, ankyrinG, Nav, and βIV spectrin—is consistent with our findings in sciatic nerves (Figure 3), suggesting that methylglyoxal exposure did not cause significant damage to CNS axons in this preparation. Furthermore, in addition to disruption of Schwann cell-mediated paranodal junctions in the PNS,

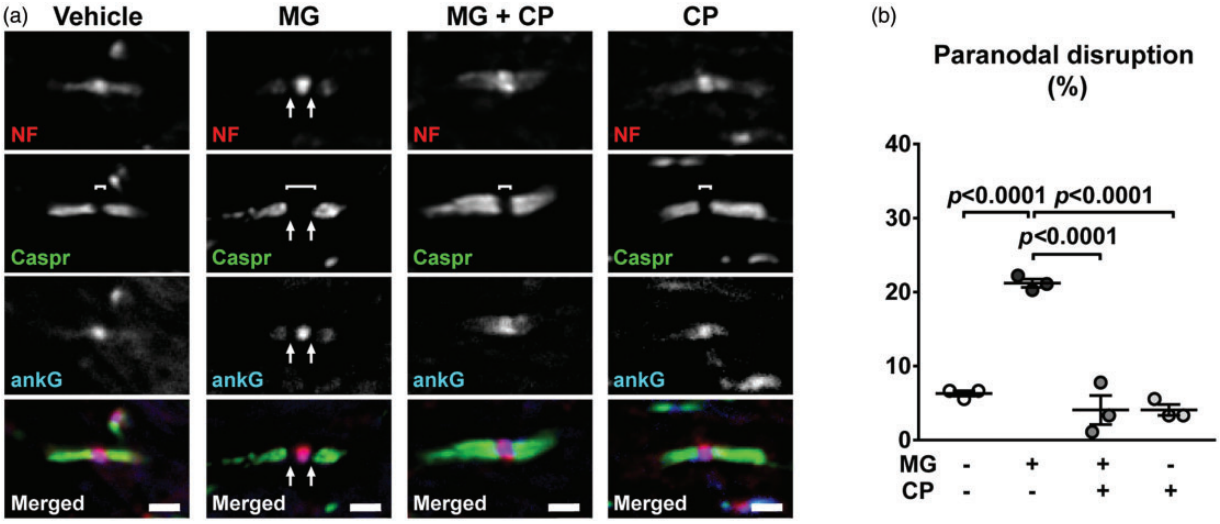

Figure 7. Calpeptin reduces methylglyoxal-evoked paranodal disruption in the CNS. (a) Exposing optic nerves to vehicle for 6 hr did not alter nodal NF186 and ankyrinG (ankG) or paranodal NF155 and Caspr immunostaining (first column). Methylglyoxal (1 mM) exposure resulted in elongation of the nodal gap (brackets) and decreased paranodal NF155 and ankyrinG staining (arrows) adjacent to the node (MG; second column). Methylglyoxal plus calpeptin exposure resulted in normal appearing nodal units (MG + CP; third column). Calpeptin treatment alone did not alter nodal unit architecture (CP; fourth column). Scale bars = 2 μm. (b) Quantification of the percentage of disrupted paranodes after exposing optic nerves to Vehicle, MG, MG + CP, or CP. Methylglyoxal-evoked paranodal disruption was ameliorated by calpeptin (two-way ANOVA followed by Tukey; n=3 nerves).

methylglyoxal disrupts oligodendrocyte-supported paranodes in the CNS.

Calpain Inhibition Prevents Methylglyoxal-Induced Paranodal Disruption in CNS

To determine if calpain inhibition prevents methylglyoxal-evoked paranodal disruption in CNS myelinated axons, we coexposed optic nerves to methylglyoxal (1 mM) and calpeptin (100 μM) for 6 hr. Paranodal NF155, Caspr, and ankyrinG as well as nodal NF186 and ankyrinG appeared normal in nerves treated with vehicle control (Figure 7(a), first column). Methylglyoxal decreased paranodal glial proteins NF155 and ankyrinG immunostaining immediately adjacent to the node, resulting in an increased length of the nodal gap between Caspr clusters (Figure 7(a), second column). This methylglyoxal-evoked paranodal disruption and apparent increase in the nodal gap length was ameliorated by calpeptin (Figure 7(a), third column). Nodal and paranodal markers in optic nerves treated with calpeptin alone appeared normal (Figure 7(a), fourth column). The apparent increase in distance between Caspr clusters after methylglyoxal exposure was ameliorated by calpeptin treatment (Figure 7(a)). Quantification of the percentage of disrupted paranodes yielded a significant interaction between methylglyoxal and calpeptin exposure, $F(1,8) = 45.74$; $p = .0001$ (Figure 7(b)). The percentage of paranodes that were disrupted by methylglyoxal ($21.2 \pm 0.56\%$, mean ± SEM, $n = 3$) was greater than that in vehicle ($6.3 \pm 0.37\%$, mean ± SEM, $n = 3$), methylglyoxal plus calpeptin ($4.1 \pm 1.96\%$, mean ± SEM, $n = 3$), or calpeptin only ($4.07 \pm 0.74\%$, mean ± SEM, $n = 3$) exposed optic nerves ($p < .0001$, two-way ANOVA followed by Tukey). Taken together, our results indicate that inhibition of calpain prevents methylglyoxal-evoked paranodal disruption in myelinated axons of both the PNS and CNS.

Discussion

Using an *ex vivo* model of acute exposure, here we show that increasing methylglyoxal levels disrupts the nodal unit in both PNS and CNS via calpain activation. Despite studies indicating the toxicity of exogenous methylglyoxal (Wang et al., 2014; Nam et al., 2015; Chan et al., 2016; Chang et al., 2016), the overall myelin structures were preserved after exposure to methylglyoxal (Figure 1(c)). Even though nerve transection in an *ex vivo* preparation initiates axonal degeneration mediated by calpain (Park et al., 2013), preservation of axonal protein clusters in both vehicle- and methylglyoxal-exposed nerves (Figure 3) suggests that 6 hr is during the latency period between nerve dissection and the initiation of axonal degeneration mechanisms (Wang et al., 2012a). Thus, our results strongly indicate that nodal unit disruption in the current study is due to experimental elevation of methylglyoxal, and not a

by-product of cell death, nerve transection, demyelination, or axonal degeneration mechanisms.

Methylglyoxal Damages Sites of Axon-Glia Interaction in Myelinated Nerves

Incubating sciatic and optic nerves with methylglyoxal resulted in disruption of both NF155 and Caspr clusters at paranodal regions immediately adjacent to the node (Figures 2 and 6), ezrin and gliomedin clusters at nodes (Figure 1), and ZO-1 clusters at paranodal autotypic junctions (Figure 1(a)). Although simultaneous loss of proteins at paranodal junctions and the extracellular matrix leads to altered nodal clusters (Feinberg et al., 2010; Susuki et al., 2013), nodal Nav channels were preserved in the current study. Previous studies suggest that nodal Nav channels are stabilized by axonal cytoskeletal and scaffolding proteins, nodal ankyrinG, and βIV spectrin, as well as paranodal βII spectrin (Ho et al., 2014; Amor et al., 2017), and we found these proteins to be preserved after methylglyoxal exposure (Figure 3). It is unclear why paranodal axoglial protein clusters were only partially affected. Perhaps a 6-hr incubation period is not long enough for complete loss of the paranode, alteration of nodal complexes, or disruption of the diffusional barrier at the paranode-juxtaparanode border that would result in Kv channel dispersion to the paranodal region, which did not occur (Figure 3(b)). Regardless, disruption of Schwann cell autotypic junctions leads to functional nerve conduction deficits (Guo et al., 2014; Hu et al., 2016) and mathematical modeling indicates that subtle retraction and partial detachment of paranodal myelin slows nerve conduction velocity (Babbs and Shi, 2013). These observations suggest that paranodal disruption induced by methylglyoxal leads to impaired action potential propagation along myelinated axons. Indeed, methylglyoxal administration *in vivo* produces nerve conduction deficits in wild-type mice (Bierhaus et al., 2012; Shimatani et al., 2015).

Methylglyoxal-Evoked Nodal Unit Disruption is Mediated by Calpain

Calpain proteases contribute to a variety of neurological diseases (Ma, 2013). Our results are the first to indicate that methylglyoxal induces calpain activation in myelinated nerve fibers. Upon pathological overactivation, calpain is reported to cleave many of the proteins that comprise functional domains of myelinated nerve fibers (Banik, 1992; Czogalla and Sikorski, 2005; Schafer et al., 2009; von Reyn et al., 2009), including axonal Nav channels, ankyrinG, and βIV spectrin. However, these axonal nodal proteins were preserved after methylglyoxal exposure (Figure 3), despite increased calpain activity (Figure 4(a)). This suggests that the observed increase in calpain activity originates in Schwann cells, not axons. Consistent with this idea, methylglyoxal disrupted the Schwann cell calpain substrates ezrin (McRobert et al., 2012) and ZO-1 (Wang et al., 2012b) (Figure 1). In the CNS, methylglyoxal reduced oligodendrocyte ankyrinG at paranodes (Figures 6 and 7), and glia-specific ablation of ankyrinG leads to delayed assembly of paranodal junction in the CNS (Chang et al., 2014). Importantly, ankyrinG is a target of calpain-mediated proteolysis (Schafer et al., 2009). Finally, calpeptin treatment prevented ezrin loss and disruption of the paranodal protein complex in PNS and CNS (Figures 5 and 7). These results taken together demonstrate that calpain mediates methylglyoxal-evoked disruption of the nodal unit, potentially through proteolysis of glial cytoskeletal scaffold.

Implications for Nervous System Pathophysiology

This study provides important clues to better understand the pathophysiology of a wide variety of diseases involving disrupted myelinated nerve fibers. For example, methylglyoxal is increased in streptozotocin-induced type 1 diabetic neuropathy (Bierhaus et al., 2012; Huang et al., 2016), and methylglyoxal-derived advanced glycation end-products are suggested to be a risk factor in the development of neuropathy in type 1 diabetic patients (Sveen et al., 2013). In addition, type 1 diabetes is associated with calcium dysregulation in the PNS (Hall et al., 2001; Verkhratsky and Fernyhough, 2014). Administering calpain inhibitors improves axonal pathology in the optic nerve (Shanab et al., 2012) or ameliorates peripheral nerve conduction deficits (Kharatmal et al., 2015) in diabetic rodents. A recent clinical report indicates significant dispersion of Caspr and NF clusters in peripheral nerves from patients with type 1 or type 2 diabetes (Doppler et al., 2017). Disruption of paranodal axoglial junctions in both peripheral nerves (Sima et al., 1986, 1988a, 1988b, 2004) and optic nerves (Sima et al., 1992; Kamijo et al., 1993) appears to be particularly associated with type 1 diabetes in patients or animal models. Furthermore, axonal excitability studies suggest that nodal and paranodal conductance are altered in the PNS of patients with type 1 diabetes even in the absence of clinical neuropathy (Kwai et al., 2016). Thus, diabetes-induced increases in methylglyoxal or calpain activation, particularly in type 1 diabetes, may be an initiator of neuropathy caused by subtle paranodal disruption.

Increased methylglyoxal (Sternberg et al., 2010, 2011) and disruption of paranodal structures (Coman et al., 2006; Howell et al., 2006) both occur in the CNS of patients with multiple sclerosis. In addition, calpain-mediated proteolysis is involved in the pathophysiology of multiple sclerosis (Shields et al., 1999), and calpeptin

treatment ameliorates optic neuritis in an animal model of multiple sclerosis-related inflammatory demyelination (Das et al., 2013). Whether a methylglyoxal-calpain mechanism contributes to paranodal disruption in multiple sclerosis remains an intriguing hypothesis.

Similar correlations between elevated methylglyoxal (Beeri et al., 2011; Fleming et al., 2011), disruption of paranodal structures (Sugiyama et al., 2002; Hinman et al., 2006), and calpain activation (Nixon, 2003) exist in the setting of aging-related neurological dysfunction. Finally, methylglyoxal is implicated in other diseases and conditions such as pain (Griggs et al., 2016, 2017a; Brings et al., 2017; Liu et al., 2017; Wei et al., 2017), anxiety (Distler and Palmer, 2012; Distler et al., 2012; McMurray et al., 2016), Alzheimer's disease (Kuhla et al., 2005, 2007), and sepsis (Brenner et al., 2014; Schmoch et al., 2017). It is unknown whether nodal units are disrupted in these conditions. Nevertheless, these studies and our current results support the idea that methylglyoxal-mediated disruption of nodal units is a pathophysiology common to many neurological diseases.

Limitations of This Study

Some of our results are not consistent with findings in human diseases or their animal models, possibly due to limitations of our *ex vivo* model. Methylglyoxal exposure did not change clusters of axonal Nav or Kv channels (Figures 3 and 6), whereas altered distribution of these channels is observed in patients or mice with type 2 diabetes (Zenker et al., 2012), patients with multiple sclerosis (Coman et al., 2006; Howell et al., 2006), or in aged animals (Hinman et al., 2006). In spontaneously diabetic BB-Wistar rats with relatively short duration of diabetes (<45 days), ezrin expression was intact and axonal Caspr and contactin as well as Schwann cell NF155 were preserved in teased sciatic nerves (Brown et al., 2001). Even though methylglyoxal is increased in patients (Bierhaus et al., 2012) or animals (Bierhaus et al., 2012; Griggs et al., 2016) with type 2 diabetes, the extent of disrupted axoglial junctions in type 2 diabetic BB/Z rats or patients was not different from their age-matched controls (Sima et al., 1988a, 2001).

A limitation of this study includes the evaluation of nodal unit pathology using an acute *ex vivo* nerve exposure model with exogenous concentrations of methylglyoxal that may exceed the physiological range. Estimates of methylglyoxal in human plasma range from 123 nM to 407 μM: and in mouse brain, estimates range from 1.5 μM to 174 μM (Rabbani and Thornalley, 2014). One study reported plasma methylglyoxal levels as high as 407 μM in diabetic patients (Lapolla et al., 2005). Intracellular levels are likely higher due to the fact that methylglyoxal is rapidly metabolized by the glyoxalase system (Allaman et al., 2015). We found a significant increase in paranodal disruption induced by 100 μM to 10 mM methylglyoxal (Figures 2(b) and 6(b)). These relatively high concentrations are necessary to achieve noticeable effects in this acute exposure model, probably because of the hematoneural diffusion barrier (Villegas et al., 2014). In addition, the relatively short duration of exposure in the current studies may not adequately reflect the disease condition of chronically elevated methylglyoxal. It would be difficult to evaluate the longer term effects of methylglyoxal on intact nerve fibers using our *ex vivo* approach because of the axonal degeneration and significant increase of calpain activation that occurs at 12 hr or later after nerve explant (Wang et al., 2012a; Park et al., 2013). Future studies using an *in vivo* model, such as via repeated systemic injection of methylglyoxal (Nigro et al., 2014; Shimatani et al., 2015; Liu et al., 2017), could overcome these limitations, and potentially lead to further dissection of methylglyoxal-evoked paranodal disruption and its complications by electron microscopy and behavioral analyses after treatment with calpain inhibitors.

Conclusions

The current results are the first to show that methylglyoxal disrupts axoglial junctions at paranodes in both PNS and CNS, alters proteins within Schwann cell microvilli or the perinodal extracellular matrix, and induces calpain activation in myelinated nerves. Our findings strongly suggest that elevated methylglyoxal in neurological diseases such as diabetic neuropathy, aging, and multiple sclerosis contributes to disruption of distinct domains along myelinated nerve fibers via calpain activation. As such, targeting calpain or methylglyoxal in specific models of these neurological diseases is a first step to developing novel treatments for impaired nervous system function.

Summary

Increasing levels of methylglyoxal drives the disruption of paranodal axoglial junctions and associated structures at the nodal functional unit that are required for normal function of the peripheral and central nervous systems. Inhibition of calpain overactivation prevents methylglyoxal-evoked paranodal disruption, suggesting that a methylglyoxal-calpain pathway mediates nervous system dysfunction in neurological diseases.

Acknowledgments

The authors thank Ms. Lulu Hong (Department of Neuroscience, Cell Biology and Physiology, Wright State University) for technical assistance, Dr. Bradley K. Taylor (Department of Physiology, University of Kentucky College of Medicine) for critical reading of the manuscript, and the

Proteome Analysis Laboratory at Wright State University for the use of equipment.

Declaration of Conflicting Interests

The author(s) declared no potential conflicts of interest with respect to the research, authorship, and/or publication of this article.

Funding

The author(s) received no financial support for the research, authorship, and/or publication of this article.

ORCID iD

Ryan B. Griggs http://orcid.org/0000-0001-7632-5897
Keiichiro Susuki http://orcid.org/0000-0002-2428-6133

References

Allaman, I., Bélanger, M., & Magistretti, P. J. (2015). Methylglyoxal, the dark side of glycolysis. *Front Neurosci*, *9*, 1–12.

Amor, V., Zhang, C., Vainshtein, A., Zhang, A., Zollinger, D. R., Eshed-Eisenbach, Y., Brophy, P. J., Rasband, M. N., & Peles, E. (2017). The paranodal cytoskeleton clusters Na+ channels at nodes of Ranvier. *Elife*, *6*, 1–15.

Andersson, D. A., Gentry, C., Light, E., Vastani, N., Vallortigara, J., Bierhaus, A., Fleming, T., & Bevan, S. (2013). Methylglyoxal evokes pain by stimulating TRPA1. *PLoS One*, *8*, 1–9.

Arancibia-Carcamo, I. L., & Attwell, D. (2014). The node of Ranvier in CNS pathology. *Acta Neuropathol*, *128*, 161–175.

Babbs, C. F., & Shi, R. (2013). Subtle paranodal injury slows impulse conduction in a mathematical model of myelinated axons. *PLoS One*, *8*, e67767.

Banik, N. L. (1992). Pathogenesis of myelin breakdown in demyelinating diseases: Role of proteolytic enzymes. *Crit Rev Neurobiol*, *6*, 257–271.

Beeri, M. S., Moshier, E., Schmeidler, J., Godbold, J., Uribarri, J., Reddy, S., Sano, M., Grossman, H. T., Cai, W., Vlassara, H., & Silverman, J. M. (2011). Serum concentration of an inflammatory glycotoxin, methylglyoxal, is associated with increased cognitive decline in elderly individuals. *Mech Ageing Dev*, *132*, 583–587.

Bhat, M. A., Rios, J. C., Lu, Y., Garcia-Fresco, G. P., Ching, W., Martin, M. S., Li, J., Einheber, S., Chesler, M., Rosenbluth, J., Salzer, J. L., & Bellen, H. J. (2001). Axon-glia interactions and the domain organization of myelinated axons requires Neurexin IV/Caspr/Paranodin. *Neuron*, *30*, 369–383.

Bi, X., Chen, J., & Baudry, M. (1998). Calpain-mediated proteolysis of GluR1 subunits in organotypic hippocampal cultures following kainic acid treatment. *Brain Res*, *781*, 355–357.

Bierhaus, A., et al. (2012). Methylglyoxal modification of Nav1.8 facilitates nociceptive neuron firing and causes hyperalgesia in diabetic neuropathy. *Nat Med*, *18*, 926–933.

Boyle, M. E. T., Berglund, E. O., Murai, K. K., Weber, L., Peles, E., & Ranscht, B. (2001). Contactin orchestrates assembly of the septate-like junctions at the paranode in myelinated peripheral nerve. *Neuron*, *30*, 385–397.

Brenner, T., Fleming, T., Uhle, F., Silaff, S., Schmitt, F., Salgado, E., Ulrich, A., Zimmermann, S., Bruckner, T., Martin, E., Bierhaus, A., Nawroth, P. P., Weigand, M. A., & Hofer, S. (2014). Methylglyoxal as a new biomarker in patients with septic shock: An observational clinical study. *Crit Care*, *18*, 683.

Brings, S., Fleming, T., De Buhr, S., Beijer, B., Lindner, T., Wischnjow, A., Kender, Z., Peters, V., Kopf, S., Haberkorn, U., Mier, W., & Nawroth, P. P. (2017). A scavenger peptide prevents methylglyoxal induced pain in mice. *Biochim Biophys Acta - Mol Basis Dis*, *1863*, 654–662.

Brown, A. A., Xu, T., Arroyo, E. J., Rock Levinson, S., Brophy, P. J., Peles, E., & Scherer, S. S. (2001). Molecular organization of the nodal region is not altered in spontaneously diabetic BB-wistar rats. *J Neurosci Res*, *65*, 139–149.

Ceccariglia, S., D'Altocolle, A., Del Fa', A., Pizzolante, F., Caccia, E., Michetti, F., & Gangitano, C. (2011). Cathepsin D plays a crucial role in the trimethyltin-induced hippocampal neurodegeneration process. *Neuroscience*, *174*, 160–170.

Chan, C. M., Huang, D. Y., Huang, Y. P., Hsu, S. H., Kang, L. Y., Shen, C. M., & Lin, W. W. (2016). Methylglyoxal induces cell death through endoplasmic reticulum stress-associated ROS production and mitochondrial dysfunction. *J Cell Mol Med*, *20*, 1749–1760.

Chang, K.-J., Zollinger, D. R., Susuki, K., Sherman, D. L., Makara, M. A., Brophy, P. J., Cooper, E. C., Bennett, V., Mohler, P. J., & Rasband, M. N. (2014). Glial ankyrins facilitate paranodal axoglial junction assembly. *Nat Neurosci*, *17*, 1673–1681.

Chang, T.-J., Tseng, H.-C., Liu, M.-W., Chang, Y.-C., Hsieh, M.-L., & Chuang, L.-M. (2016). Glucagon-like peptide-1 prevents methylglyoxal-induced apoptosis of beta cells through improving mitochondrial function and suppressing prolonged AMPK activation. *Sci Rep*, *6*, 23403.

Choi, Y. Y., Kim, S., Han, J. H., Nam, D. H., Park, K. M., Kim, S. Y., & Woo, C. H. (2016). CHOP deficiency inhibits methylglyoxal-induced endothelial dysfunction. *Biochem Biophys Res Commun*, *480*, 362–368.

Coman, I., Aigrot, M. S., Seilhean, D., Reynolds, R., Girault, J. A., Zalc, B., & Lubetzki, C. (2006). Nodal, paranodal and juxtaparanodal axonal proteins during demyelination and remyelination in multiple sclerosis. *Brain*, *129*, 3186–3195.

Czogalla, A., & Sikorski, A. F. (2005). Spectrin and calpain: A "target" and a "sniper" in the pathology of neuronal cells. *Cell Mol Life Sci*, *62*, 1913–1924.

Das, A., Guyton, M. K., Smith, A., Wallace, G., McDowell, M. L., Matzelle, D. D., Ray, S. K., & Banik, N. L. (2013). Calpain inhibitor attenuated optic nerve damage in acute optic neuritis in rats. *J Neurochem*, *124*, 133–146.

Distler, M. G., & Palmer, A. A. (2012). Role of glyoxalase 1 (Glo1) and methylglyoxal (MG) in behavior: Recent advances and mechanistic insights. *Front Genet*, *3*, 1–10.

Distler, M. G., Plant, L. D., Sokoloff, G., Hawk, A. J., Aneas, I., Wuenschell, G. E., Termini, J., Meredith, S. C., Nobrega, M. A., & Palmer, A. A. (2012). Glyoxalase 1 increases

anxiety by reducing GABA A receptor agonist methylglyoxal. *J Clin Invest*, *122*, 2306–2315.

Doppler, K., Frank, F., Koschker, A.-C., Reiners, K., & Sommer, C. (2017). Nodes of Ranvier in skin biopsies of patients with diabetes mellitus. *J Peripher Nerv Syst*, *190*, 182–190.

Eberhardt, M. J., Filipovic, M. R., Leffler, A., De La Roche, J., Kistner, K., Fischer, M. J., Fleming, T., Zimmermann, K., Ivanovic-Burmazovic, I., Nawroth, P. P., Bierhaus, A., Reeh, P. W., & Sauer, S. K. (2012). Methylglyoxal activates nociceptors through transient receptor potential channel A1 (TRPA1): A possible mechanism of metabolic neuropathies. *J Biol Chem*, *287*, 28291–28306.

Eshed, Y., Feinberg, K., Carey, D. J., & Peles, E. (2007). Secreted gliomedin is a perinodal matrix component of peripheral nerves. *J Cell Biol*, *177*, 551–562.

Feinberg, K., Eshed-Eisenbach, Y., Frechter, S., Amor, V., Salomon, D., Sabanay, H., Dupree, J. L., Grumet, M., Brophy, P. J., Shrager, P., & Peles, E. (2010). A glial signal consisting of gliomedin and NrCAM clusters axonal Na+ channels during the formation of nodes of Ranvier. *Neuron*, *65*, 490–502.

Fleming, T. H., Humpert, P. M., Nawroth, P. P., & Bierhaus, A. (2011). Reactive metabolites and AGE/RAGE-mediated cellular dysfunction affect the aging process—A mini-review. *Gerontology*, *57*, 435–443.

Griggs, R. B., Donahue, R. R., Adkins, B. G., Anderson, K. L., Thibault, O., & Taylor, B. K. (2016). Pioglitazone inhibits the development of hyperalgesia and sensitization of spinal nociresponsive neurons in type 2 diabetes. *J Pain*, *17*, 359–373.

Griggs, R. B., Laird, D. E., Donahue, R. R., Fu, W., & Taylor, B. K. (2017a). Methylglyoxal requires AC1 and TRPA1 to produce pain and spinal neuron activation. *Front Neurosci*, *11*, 1–11.

Griggs, R. B., Yermakov, L. M., & Susuki, K. (2017b). Formation and disruption of functional domains in myelinated CNS axons. *Neurosci Res*, *116*, 77–87.

Guo, J., Wang, L., Zhang, Y., Wu, J., Arpag, S., Hu, B., Imhof, B. A., Tian, X., Carter, B. D., Suter, U., & Li, J. (2014). Abnormal junctions and permeability of myelin in PMP22-deficient nerves. *Ann Neurol*, *75*, 255–265.

Hall, K. E., Liu, J., Sima, A. A. F., & Wiley, J. W. (2001). Impaired inhibitory G-protein function contributes to increased calcium currents in rats with diabetic neuropathy. *J Neurophysiol*, *86*, 760–770.

Hinman, J. D., Peters, A., Cabral, H., Rosene, D. L., Hollander, W., Rasband, M. N., & Abraham, C. R. (2006). Age-related molecular reorganization at the node of Ranvier. *J Comp Neurol*, *495*, 351–362.

Ho, T. S.-Y., Zollinger, D. R., Chang, K.-J., Xu, M., Cooper, E. C., Stankewich, M. C., Bennett, V., & Rasband, M. N. (2014). A hierarchy of ankyrin-spectrin complexes clusters sodium channels at nodes of Ranvier. *Nat Neurosci*, *17*, 1664–1672.

Howell, O. W., Palser, A., Polito, A., Melrose, S., Zonta, B., Scheiermann, C., Vora, A. J., Brophy, P. J., & Reynolds, R. (2006). Disruption of neurofascin localization reveals early changes preceding demyelination and remyelination in multiple sclerosis. *Brain*, *129*, 3173–3185.

Hu, B., Arpag, S., Zhang, X., Mobius, W., Werner, H., Sosinsky, G., Ellisman, M., Zhang, Y., Hamilton, A., Chernoff, J., & Li, J. (2016). Tuning PAK activity to rescue abnormal myelin permeability in HNPP. *PLoS Genet*, *12*, 1–24.

Huang, Q., Chen, Y., Gong, N., & Wang, Y. X. (2016). Methylglyoxal mediates streptozotocin-induced diabetic neuropathic pain via activation of the peripheral TRPA1 and Nav1.8 channels. *Metabolism*, *65*, 463–474.

Kamijo, M., Cherian, P. V., & Sima, A. A. F. (1993). The preventive effect of aldose reductase inhibition on diabetic optic neuropathy in the BB/W-rat. *Diabetol Clin Exp Diabetes Metab*, *36*, 893–898.

Kharatmal, S. B., Singh, J. N., & Sharma, S. S. (2015). Calpain inhibitor, MDL 28170 confer electrophysiological, nociceptive and biochemical improvement in diabetic neuropathy. *Neuropharmacology*, *97*, 113–121.

Kuhla, B., Boeck, K., Schmidt, A., Ogunlade, V., Arendt, T., Münch, G., & Lüth, H. J. (2007). Age- and stage-dependent glyoxalase I expression and its activity in normal and Alzheimer's disease brains. *Neurobiol Aging*, *28*, 29–41.

Kuhla, B., Lüth, H. J., Haferburg, D., Boeck, K., Arendt, T., & Münch, G. (2005). Methylglyoxal, glyoxal, and their detoxification in Alzheimer's disease. *Ann N Y Acad Sci*, *1043*, 211–216.

Kwai, N. C. G., Arnold, R., Poynten, A. M., Howells, J., Kiernan, M. C., Lin, C. S. Y., & Krishnan, A. V. (2016). In vivo evidence of reduced nodal and paranodal conductances in type 1 diabetes. *Clin Neurophysiol*, *127*, 1700–1706.

Lapolla, A., Reitano, R., Seraglia, R., Sartore, G., Ragazzi, E., & Traldi, P. (2005). Evaluation of advanced glycation end products and carbonyl compounds in patients with different conditions of oxidative stress. *Mol Nutr Food Res*, *49*, 685–690.

Li, W., Maloney, R. E., Circu, M. L., Alexander, J. S., & Aw, T. Y. (2013). Acute carbonyl stress induces occludin glycation and brain microvascular endothelial barrier dysfunction: Role for glutathione-dependent metabolism of methylglyoxal. *Free Radic Biol Med*, *54*, 51–61.

Liu, C.-C., Zhang, X.-S., Ruan, Y.-T., Huang, Z.-X., Zhang, S.-B., Liu, M., Luo, H.-J., Wu, S.-L., & Ma, C. (2017). Accumulation of methylglyoxal increases the advanced glycation end products levels in DRG and contributes to lumbar disc herniation-induced persistent pain. *J Neurophysiol*, *118*, 1321–1328.

Ma, M. (2013). Role of calpains in the injury-induced dysfunction and degeneration of the mammalian axon. *Neurobiol Dis*, *60*, 61–79.

McMurray, K. M. J., Du, X., Brownlee, M., & Palmer, A. A. (2016). Neuronal overexpression of Glo1 or amygdalar microinjection of methylglyoxal is sufficient to regulate anxiety-like behavior in mice. *Behav Brain Res*, *301*, 119–123.

McRobert, E. A., Young, A. N., & Bach, L. A. (2012). Advanced glycation end-products induce calpain-mediated degradation of ezrin. *FEBS J*, *279*, 3240–3250.

Melendez-Vasquez, C. V., Rios, J. C., Zanazzi, G., Lambert, S., Bretscher, A., & Salzer, J. L. (2001). Nodes of Ranvier form in association with ezrin-radixin-moesin (ERM)-positive Schwann cell processes. *Proc Natl Acad Sci U S A*, *98*, 1235–1240.

Nam, D. H., Han, J. H., Lee, T. J., Shishido, T., Lim, J. H., Kim, G. Y., & Woo, C. H. (2015). CHOP deficiency prevents methylglyoxal-induced myocyte apoptosis and cardiac dysfunction. *J Mol Cell Cardiol*, *85*, 168–177.

Nigro, C., Raciti, G. A., Leone, A., Fleming, T. H., Longo, M., Prevenzano, I., Fiory, F., Mirra, P., D'Esposito, V., Ulianich, L., Nawroth, P. P., Formisano, P., Beguinot, F., & Miele, C. (2014). Methylglyoxal impairs endothelial insulin sensitivity both in vitro and in vivo. *Diabetologia*, *57*, 1485–1494.

Nixon, R. A. (2003). The calpains in aging and aging-related diseases. *Ageing Res Rev*, *2*, 407–418.

Otani, Y., Yermakov, L. M., Dupree, J. L., & Susuki, K. (2017). Chronic peripheral nerve compression disrupts paranodal axoglial junctions. *Muscle Nerve*, *55*, 544–554.

Palsamy, P., Bidasee, K. R., Ayaki, M., Augusteyn, R. C., Chan, J. Y., & Shinohara, T. (2014). Methylglyoxal induces endoplasmic reticulum stress and DNA demethylation in the Keap1 promoter of human lens epithelial cells and age-related cataracts. *Free Radic Biol Med*, *72*, 134–148.

Park, J. Y., Jang, S. Y., Shin, Y. K., Suh, D. J., & Park, H. T. (2013). Calcium-dependent proteasome activation is required for axonal neurofilament degradation. *Neural Regen Res*, *8*, 3401–3409.

Pillai, A. M., Thaxton, C., Pribisko, A. L., Cheng, G., Dupree, J. L., & Bhat, M. A. (2009). Spatiotemporal ablation of myelinating glia-specific neurofascin (NfascNF155) in mice reveals gradual loss of paranodal axoglial junctions and concomitant disorganization of axonal domains. *J Neurosci Res*, *87*, 1773–1793.

Poliak, S., Matlis, S., Ullmer, C., Scherer, S. S., & Peles, E. (2002). Distinct claudins and associated PDZ proteins form different autotypic tight junctions in myelinating Schwann cells. *J Cell Biol*, *159*, 361–371.

Rabbani, N., & Thornalley, P. J. (2014). Measurement of methylglyoxal by stable isotopic dilution analysis LC-MS/MS with corroborative prediction in physiological samples. *Nat Protoc*, *9*, 1969–1979.

Rosca, M. G., Monnier, V. M., Szweda, L. I., & Weiss, M. F. (2002). Alterations in renal mitochondrial respiration in response to the reactive oxoaldehyde methylglyoxal. *Am J Physiol Renal Physiol*, *283*, F52–F59.

Schafer, D. P., Jha, S., Liu, F., Akella, T., McCullough, L. D., & Rasband, M. N. (2009). Disruption of the axon initial segment cytoskeleton is a new mechanism for neuronal injury. *J Neurosci*, *29*, 13242–13254.

Schmoch, T., Uhle, F., Siegler, B. H., Fleming, T., Morgenstern, J., Nawroth, P. P., Weigand, M. A., & Brenner, T. (2017). The glyoxalase system and methylglyoxal-derived carbonyl stress in sepsis: Glycotoxic aspects of sepsis pathophysiology. *Int J Mol Sci*, *18*, 1–19.

Shanab, A. Y., Nakazawa, T., Ryu, M., Tanaka, Y., Himori, N., Taguchi, K., Yasuda, M., Watanabe, R., Takano, J., Saido, T., Minegishi, N., Miyata, T., Abe, T., & Yamamoto, M. (2012). Metabolic stress response implicated in diabetic retinopathy: The role of calpain, and the therapeutic impact of calpain inhibitor. *Neurobiol Dis*, *48*, 556–567.

Shi, Y., Sun, W., McBride, J. J., Cheng, J. X., & Shi, R. (2011). Acrolein induces myelin damage in mammalian spinal cord. *J Neurochem*, *117*, 554–564.

Shields, D. C., Schaecher, K. E., Saido, T. C., & Banik, N. L. (1999). A putative mechanism of demyelination in multiple sclerosis by a proteolytic enzyme, calpain. *Proc Natl Acad Sci U S A*, *96*, 11486–11491.

Shimatani, Y., Nodera, H., Osaki, Y., Banzrai, C., Takayasu, K., Endo, S., Shibuta, Y., & Kaji, R. (2015). Upregulation of axonal HCN current by methylglyoxal: Potential association with diabetic polyneuropathy. *Clin Neurophysiol*, *126*, 2226–2232.

Sima, A. A. F., Lattimer, S. A., Yagihashi, S., & Greene, D. A. (1986). Axo-glial dysjunction. A novel structural lesion that accounts for poorly reversible slowing of nerve conduction in the spontaneously diabetic bio-breeding rat. *J Clin Invest*, *77*, 474–484.

Sima, A. A. F., Nathaniel, V., Bril, V., McEwen, T. A. J., & Greene, D. A. (1988a). Histopathological heterogeneity of neuropathy in insulin-dependent and non-insulin-dependent diabetes, and demonstration of axo-glial dysjunction in human diabetic neuropathy. *J Clin Invest*, *81*, 349–364.

Sima, A. A. F., Zhang, W., Li, Z. G., Murakawa, Y., & Pierson, C. R. (2004). Molecular alterations underlie nodal and paranodal degeneration in type 1 diabetic neuropathy and are prevented by C-peptide. *Diabetes*, *53*, 1556–1563.

Sima, A. A. F., Zhang, W., Sugimoto, K., Henry, D., Li, Z., Wahren, J., & Grunberger, G. (2001). C-peptide prevents and improves chronic type I diabetic polyneuropathy in the BB/Wor rat. *Diabetologia*, *44*, 889–897.

Sima, A. A. F., Zhang, W., Tze, W. A. H. J., Tai, J., & Nathaniel, V. (1988b). Diabetic neuropathy in STZ-induced diabetic rat and effect of allogeneic islet cell transplantation morphometric analysis. *Diabetes*, *37*, 1129–1136.

Sima, A. A. F., Zhang, W. X., Cherian, P. V., & Chakrabarti, S. (1992). Impaired visual evoked potential and primary axonopathy of the optic nerve in the diabetic BB/W-rat. *Diabetologia*, *35*, 602–607.

Sternberg, Z., Hennies, C., Sternberg, D., Wang, P., Kinkel, P., Hojnacki, D., Weinstock-Guttmann, B., & Munschauer, F. (2010). Diagnostic potential of plasma carboxymethyllysine and carboxyethyllysine in multiple sclerosis. *J Neuroinflammation*, *7*, 72.

Sternberg, Z., Ostrow, P., Vaughan, M., Chichelli, T., & Munschauer, F. (2011). AGE-RAGE in multiple sclerosis brain. *Immunol Invest*, *40*, 197–205.

Sugiyama, I., Tanaka, K., Akita, M., Yoshida, K., Kawase, T., & Asou, H. (2002). Ultrastructural analysis of the paranodal junction of myelinated fibers in 31-month-old-rats. *J Neurosci Res*, *70*, 309–317.

Susuki, K. (2013). Node of Ranvier disruption as a cause of neurological diseases. *ASN Neuro*, *5*, 209–219.

Susuki, K., Chang, K. J., Zollinger, D. R., Liu, Y., Ogawa, Y., Eshed-Eisenbach, Y., Dours-Zimmermann, M. T.,

Oses-Prieto, J. A., Burlingame, A. L., Seidenbecher, C. I., Zimmermann, D. R., Oohashi, T., Peles, E., & Rasband, M. N. (2013). Three mechanisms assemble central nervous system nodes of ranvier. *Neuron*, *78*, 469–482.

Sveen, K. A., Karimé, B., Jørum, E., Mellgren, S. I., Fagerland, M. W., Monnier, V. M., Dahl-Jørgensen, K., & Hanssen, K. F. (2013). Small- and large-fiber neuropathy after 40 years of type 1 diabetes: Associations with glycem ic control andadvanced protein glycation: The Oslo Study. *Diabetes Care*, *36*, 3712–3717.

Tajes, M., Eraso-Pichot, A., Rubio-Moscardó, F., Guivernau, B., Bosch-Morató, M., Valls-Comamala, V., & Muñoz, F. J. (2014). Methylglyoxal reduces mitochondrial potential and activates Bax and caspase-3 in neurons: Implications for Alzheimer's disease. *Neurosci Lett*, *580*, 78–82.

Verkhratsky, A., & Fernyhough, P. (2014). Calcium signalling in sensory neurones and peripheral glia in the context of diabetic neuropathies. *Cell Calcium*, *56*, 362–371.

Villegas, R., Martinez, N. W., Lillo, J., Pihan, P., Hernandez, D., Twiss, J. L., & Court, F. A. (2014). Calcium release from intra-axonal endoplasmic reticulum leads to axon degeneration through mitochondrial dysfunction. *J Neurosci*, *34*, 7179–7189.

von Reyn, C. R., Spaethling, J. M., Mesfin, M. N., Ma, M., Neumar, R. W., Smith, D. H., Siman, R., & Meaney, D. F. (2009). Calpain mediates proteolysis of the voltage-gated sodium channel alpha-subunit. *J Neurosci*, *29*, 10350–10356.

Vosler, P. S., Brennan, C. S., & Chen, J. (2008). Calpain-mediated signaling mechanisms in neuronal injury and neurodegeneration. *Mol Neurobiol*, *38*, 78–100.

Wang, J. T., Medress, Z. A., & Barres, B. A. (2012a). Axon degeneration: Molecular mechanisms of a self-destruction pathway. *J Cell Biol*, *196*, 7–18.

Wang, T., Wang, L., Moreno-Vinasco, L., Lang, G. D., Siegler, J. H., Mathew, B., Usatyuk, P. V., Samet, J. M., Geyh, A. S., Breysse, P. N., Natarajan, V., & Garcia, J. G. N. (2012b). Particulate matter air pollution disrupts endothelial cell barrier via calpain-mediated tight junction protein degradation. *Part Fibre Toxicol*, *9*, 35.

Wang, Y. H., Yu, H. T., Pu, X. P., & Du, G. H. (2014). Myricitrin alleviates methylglyoxal-induced mitochondrial dysfunction and AGEs/RAGE/NF-κB pathway activation in SH-SY5Y cells. *J Mol Neurosci*, *53*, 562–570.

Wei, J.-Y., Liu, C.-C., Ouyang, H.-D., Ma, C., Xie, M.-X., Liu, M., Lei, W.-L., Ding, H.-H., Wu, S.-L., Xin, W.-J. (2017). Activation of RAGE/STAT3 pathway by methylglyoxal contributes to spinal central sensitization and persistent pain induced by bortezomib. *Exp Neurol*, *296*, 74–82.

Wetzels, S., Wouters, K., Schalkwijk, C., Vanmierlo, T., & Hendriks, J. (2017). Methylglyoxal-derived advanced glycation endproducts in multiple sclerosis. *Int J Mol Sci*, *18*, 421.

Zenker, J., Poirot, O., de Preux Charles, A.-S., Arnaud, E., Medard, J.-J., Lacroix, C., Kuntzer, T., & Chrast, R. (2012). Altered distribution of juxtaparanodal Kv1.2 subunits mediates peripheral nerve hyperexcitability in type 2 diabetes mellitus. *J Neurosci*, *32*, 7493–7498.

Zhang, C., Deng, Y., Dai, H., Zhou, W., Tian, J., Bing, G., & Zhao, L. (2017). Effects of dimethyl sulfoxide on the morphology and viability of primary cultured neurons and astrocytes. *Brain Res Bull*, *128*, 34–39.